First-principles calculation of the effective on-site Coulomb interaction parameters for Sr_2ABO_6 (A=Cr, Mn, Fe, Co, Ni, and B=Mo, W) double perovskites

A. Neroni,[1] E. Şaşıoğlu,[2,1,*] H. Hadipour,[3] C. Friedrich,[1] S. Blügel,[1] I. Mertig,[2] and M. Ležaić[1]

[1]*Peter Grünberg Institut and Institute for Advanced Simulation, Forschungszentrum Jülich and JARA, 52425 Jülich, Germany*

[2]*Institute of Physics, Martin Luther University Halle-Wittenberg, 06120 Halle (Saale), Germany*

[3]*Department of Physics, University of Guilan, 41335-1914 Rasht, Iran*

(Received 14 November 2017; revised manuscript received 18 July 2019; published 6 September 2019)

Double perovskites (DPs) are a large family of compounds that exhibit a wide range of properties of both fundamental and potential technological interest. Due to the presence of $3d$, $4d$, or $5d$ transition metal atoms with narrow t_{2g} and e_g bands in DPs, the correlation effects play an important role for the properties of these materials, leading to diverse physical phenomena, such as colossal magnetoresistance, ferroelectricity, magnetism, and superconductivity. By employing the constrained random-phase approximation within the full-potential linearized augmented-plane-wave method, we have calculated the effective on-site Coulomb interaction parameters between localized d electrons in Sr_2ABO_6 (A = Cr, Mn, Fe, Co, Ni, and B = Mo, W) DPs. We find that the correlated subspace can be defined to contain only the e_g states in Ni-based compounds, leading to a simple two-band low-energy model, whereas at least an eight-orbital ($d + t_{2g}$) model is necessary for the other compounds. Except for Ni, the U values for A sites in Mo (W) based compounds are around 4 eV (4.5 eV), and they are almost independent of the $3d$ electron number, while the U for Mo (W) t_{2g} electrons slightly decreases with increasing $3d$ electron number, from 3 to 2.5 eV. Moreover, our calculations reveal that the contribution of the $3d \rightarrow 3d$ channel to the total electronic screening is larger in DPs than the corresponding contribution in elementary transition metals.

DOI: 10.1103/PhysRevB.100.115113

I. INTRODUCTION

Double perovskites (DPs) show incredibly rich physical properties owing to the huge variety of elements that can be combined [1]. Ferrimagnetism above room temperature was first reported in Re- and Os-based systems [2,3]. Since then, other DP compounds have been found to show magnetic orderings ranging from ferromagnetism to ferrimagnetism and antiferromagnetism. Beside metallic and insulating compounds, notably half-metallic DPs such as Sr_2FeMoO_6 (SFMO) have been found. Experimentally, SFMO is reported as a ferrimagnetic half metal. The possibility of 100% spin polarization is very important in the field of spintronic applications. Other interesting properties of DPs include colossal magnetoresistance, presence of ferroelectricity, and superconductivity at high temperatures [4–7]. The presence of both half metallicity and perfectly compensated ferrimagnetism in a single material has even been anticipated to lead to single-spin superconductivity [8]. Moreover, the extensive tunability of the physical properties of DPs through chemical substitutions makes the family especially interesting.

Due to the presence of $3d$, $4d$, or $5d$ transition metal atoms with narrow t_{2g} and e_g bands, correlation effects play an important role in the DPs. In calculations utilizing density functional theory (DFT), the DFT+U method has been used to obtain electronic, magnetic, and optical properties of several DP compounds [9–16]. In the literature, it is common to use a "standard" value for the Hubbard U parameter, usually taken from the values found for other compounds containing the same transition metal ion. However, this approach does not give satisfactory results when compared to experiments. It has been shown, for example, that there is a strong dependence of the spin-phonon coupling effects on the Hubbard U in both single and double perovskites [12]. Only recently, refined approaches such as DFT+DMFT (dynamical mean-field theory) have been used for Sr_2YIrO_6 and Ba_2YIrO6, with Hubbard U parameters obtained from *ab initio* calculations to study their electronic and magnetic structures [14]. These recent works suggest that a fully *ab initio* treatment is highly desirable to avoid bias in the determination of complex physical properties of DPs.

The *ab initio* determination of the effective Coulomb interaction parameters for transition metals (TMs) and their compounds was already addressed by several authors employing different methods [17–33]. The earliest approach, the constrained local-density approximation (cLDA) [20–22], is still in wide use even though it is known to deliver unreasonably large U and J values especially for late TMs. Moreover, since the Hubbard U is, within this approach, calculated in the framework of DFT, its frequency dependence cannot be obtained. The constrained random-phase approximation (cRPA) is an approach that, though numerically much more demanding, does not suffer from these deficiencies. In contrast to cLDA, the cRPA also allows individual Coulomb matrix elements to be accessed, e.g., on-site, off-site, intraorbital, interorbital, and exchange elements. The frequency dependence gives access to the study of dynamical properties [23,27].

*ersoy.sasioglu@physik.uni-halle.de

The aim of the present work is to identify suitable correlated subspaces and present a systematic study of the effective on-site Coulomb interaction parameters for the d electrons in Sr_2ABO_6 (A = Cr, Mn, Fe, Co, Ni, and B = Mo, W) DPs. Employing the cRPA approach within the full-potential linearized augmented-plane-wave (FLAPW) method, we have determined the effective on-site Coulomb interaction parameters in a series of 10 DPs. We consider the constrained non-spin-polarized (nonmagnetic) and the spin-polarized ground states of the DPs. For the nonmagnetic state, we find U values around 4 eV (4.5 eV) for the A sites except A = Ni in Mo (W) based compounds, almost independent of the $3d$ electron number. On the other hand, the U values for Mo and W t_{2g} orbitals slightly decrease with increasing $3d$ electron number, from 3 to 2.5 eV. For the spin-polarized case, the U parameters show some variations due to the exchange splitting and a redistribution of the states around Fermi energy, but the overall trend is similar to the nonmagnetic state. Moreover, our calculations reveal that the contribution of the $3d \rightarrow 3d$ channel to the total electronic screening is stronger in DPs than in the case of the elementary transition metals. We show that all DPs, except the Ni-based ones, can be described by an eight-orbital effective low-energy model. The calculated U parameters are not only important for a fundamental understanding of the physics of DPs, but they can also serve as effective interaction parameters to be used in model Hamiltonians applied to describe electronic, optical, and magnetic properties. This provides model parameters from first principles rather than having to fit them to experimental data, thus increasing the predictive power of model calculations.

The rest of the paper is organized as follows. In Sec. II, we briefly present the computational method. In Sec. III, we present calculated values of Coulomb interaction parameters for two series of DPs, with electronic properties ranging from insulator to half metal and to metal, depending on the filling of the $3d$ shell. Finally, we summarize our conclusions in Sec. IV.

II. COMPUTATIONAL METHOD

DPs represent a step further in complexity from simple perovskites and crystallize in a cubic structure as shown in Fig. 1. Two perovskite unit cells are combined to form compounds in which several stacking patterns of different cations give rise to complicated structures whose general formula unit is X_2ABO_6 [34]. As for simple perovskites, the basic unit cell is cubic, but very often distortions are present, such as an elongation of lattice vectors, and tilting and deforming of the oxygen octahedra. In the case of DPs with a rocksalt type of ordering of the two present cations, the DPs are described by a unit cell shown in Fig. 1. The X cations occupy the positions $\{\frac{1}{2}, 0, \frac{1}{4}\}$, $\{\frac{1}{2}, 0, \frac{3}{4}\}$, $\{0, \frac{1}{2}, \frac{1}{4}\}$, and $\{0, \frac{1}{2}, \frac{3}{4}\}$. The A cations occupy positions $\{0, 0, 0\}$, $\{\frac{1}{2}, \frac{1}{2}, \frac{1}{2}\}$, while the B cations are at $\{\frac{1}{2}, \frac{1}{2}, 0\}$ and $\{0, 0, \frac{1}{2}\}$. The cations A and B are surrounded by octahedral oxygen cages, and the AO_6 and BO_6 groups are arranged in two interpenetrating fcc sublattices. Here, we consider a series of ten DPs with formulas Sr_2ABO_6 where A = (Cr, Mn, Fe, Co, Ni) and B = (Mo, W). Their lattice parameters are taken from Ref. [1] and presented in Table I. In order to obtain the trends with increasing number of electrons in the studied DP series, all calculations have been performed for the ideal cubic structure with the unit cell comprising ten atoms, without taking into account the relaxation of the internal coordinates of the ions, or possible distortions specific to each of the compounds. Moreover, while the distortions in DPs can lead to shifts of the Fermi level, E_F, and even to a metal-to-insulator transition, we note that E_F remains within the d manifold. As we observe the screening of the d states by all the other states, we therefore do not expect the effect of the deformations to be very strong, especially in the case of the unscreened U.

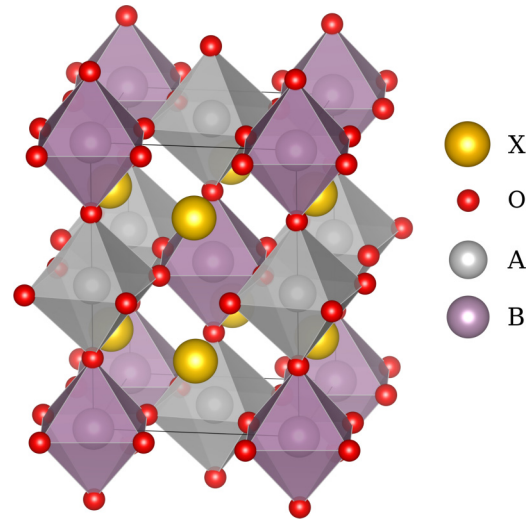

FIG. 1. Cubic double-perovskite structure for the general formula X_2ABO_6 used in this work.

The FLAPW method as implemented in the FLEUR code [35] is used for the constrained non-spin-polarized (nonmagnetic) as well as for the spin-polarized ground-state calculations. We employ the generalized gradient approximation (GGA) to the exchange-correlation potential as parametrized

TABLE I. Lattice parameters (in Å), atom-resolved and total magnetic moments (in μ_B), and ground state (GS) for the two series Sr_2AMoO_6 and Sr_2AWO_6.

			Sr_2AMoO_6		
A	a	$m^{[A]}$	$m^{[Mo]}$	$m^{[Cell]}$	GS
Cr	7.84	2.30	−0.44	2.00	Half metal
Mn	7.96	3.14	−0.51	2.71	Ferrimagnetic metal
Fe	7.90	3.79	−0.31	4.00	Half metal
Co	8.09	2.70	−0.18	3.00	Half metal
Ni	7.89	1.59	0.06	2.00	Magnetic insulator
			Sr_2AWO_6		
A	a	$m^{[A]}$	$m^{[W]}$	$m^{[Cell]}$	GS
Cr	7.81	2.23	−0.35	2.00	Half metal
Mn	8.02	3.55	−0.24	3.51	Ferrimagnetic metal
Fe	7.94	3.74	−0.20	4.00	Half metal
Co	8.14	2.67	−0.08	3.00	Half metal
Ni	7.92	1.61	0.06	2.00	Magnetic insulator

by Perdew *et al.* [36]. To keep the trends in the results consistent, calculations have been performed using the same value for the cutoff of the wave functions ($k_{\max} = 4$ a.u.$^{-1}$) and the same $10 \times 10 \times 10$ k-point grid in the determination of the ground states. We have checked that these parameters yield well-converged Coulomb interaction parameters in all the studied compounds. The maximally localized Wannier functions (MLWFs) are constructed with the WANNIER90 library [37–39]. The Ni-based DPs show well-isolated e_g bands at the Fermi energy [see Fig. 2(b)], which motivates a simple two-band model for these compounds with e_g Wannier orbitals. In the other DPs, the e_g states for the B-site cations are well separated from the t_{2g} states and are located 4–5 eV above the Fermi energy. Thus, we construct Wannier functions for the $3d$ orbitals at the A-site cations and for the t_{2g} orbitals at the B-site cations (see Fig. 2). These states are mainly responsible for the electronic, magnetic, and transport properties of the DPs. In the nonmagnetic state, they are disentangled from the other bands of O p and Sr s character, giving an eight-band model. Note that in spin-polarized calculations the t_{2g} bands of the A-site cations are weakly entangled with the O p bands in some parts of the Brillouin zone [see Fig. 2(c)], which is why we included a few more states in construction of the Wannier functions. The effective Coulomb potential is calculated within the cRPA method [23,25,26] implemented in the SPEX code [40] (for further technical details see Refs. [27,41]). We use a $5 \times 5 \times 5$ k-point grid in the cRPA calculations.

In the cRPA approach, the full polarization matrix P is divided into two parts: $P = P_d + P_r$, where P_d includes only d-d transitions and P_r is the remainder. Then, the frequency-dependent effective Coulomb interaction is given schematically by the matrix equation $U(\omega) = [1 - vP_r(\omega)]^{-1}v$, where v is the bare Coulomb interaction and $U(\omega)$ is related to the fully screened interaction by $\tilde{U}(\omega) = [1 - U(\omega)P_d(\omega)]^{-1}U(\omega)$. In the paramagnetic state, the correlated subspace P_d is well defined for all compounds: From $A =$ Cr to $A =$ Co it contains A-site cation $3d$ ($t_{2g} + e_g$) and Mo (W) t_{2g} states, which are disentangled from the rest of the Hilbert space, whereas the subspace only consists of the Ni e_g states in the Ni-based compounds. In Figs. 2(a) and 2(b), we show the correlated subspaces for paramagnetic Sr_2FeMoO_6 and Sr_2NiMoO_6. For comparison, the spin-polarized correlated subspace for Sr_2FeMoO_6 is presented in Figs. 2(c) and 2(d). Note that in the paramagnetic state all compounds except Sr_2FeMoO_6 possess correlated states crossing the Fermi energy. The comparison of the DFT-PBE band structure (see Fig. 2) with Wannier interpolated bands reveals that the correlated subspace can be well represented by a minimal number of Wannier orbitals in a model Hamiltonian description of the DPs. In Fig. 3, we visualize the t_{2g}- and e_g-like Wannier orbitals for paramagnetic Sr_2FeMoO_6. As seen, Wannier orbitals are well localized on atomic sites.

We consider matrix elements of U in the MLWF basis:

$$U^{\sigma_1,\sigma_2}_{in_1,jn_3,in_2,jn_4}(\omega) = \iint d\boldsymbol{r}d\boldsymbol{r}'\, w^{\sigma_1 *}_{in_1}(\boldsymbol{r}) w^{\sigma_2 *}_{jn_3}(\boldsymbol{r}') U(\boldsymbol{r},\boldsymbol{r}',\omega) w^{\sigma_2}_{jn_4}(\boldsymbol{r}') w^{\sigma_1}_{in_2}(\boldsymbol{r}). \quad (1)$$

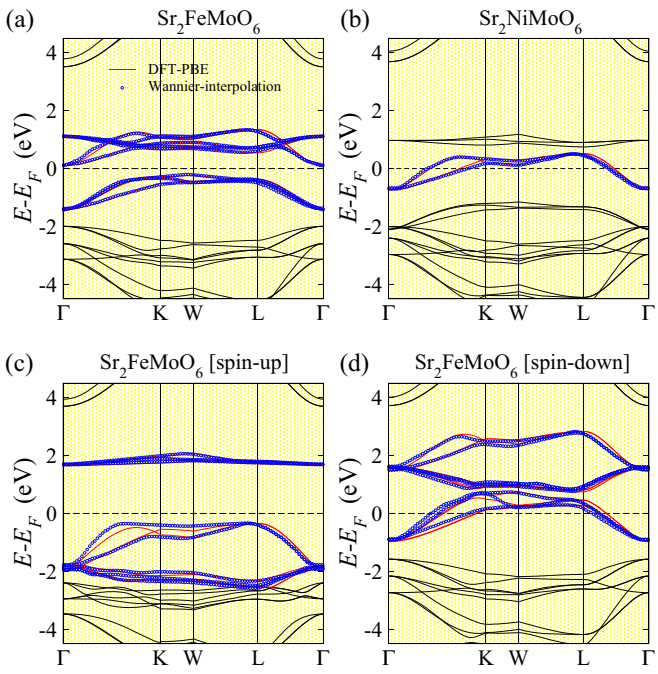

FIG. 2. DFT-PBE and Wannier-interpolated band structure of nonmagnetic (a) Sr_2FeMoO_6 and (b) Sr_2NiMoO_6. (c) and (d) The same as (a) for the spin-polarized case. Dashed lines denote the Fermi energy, which is set to zero.

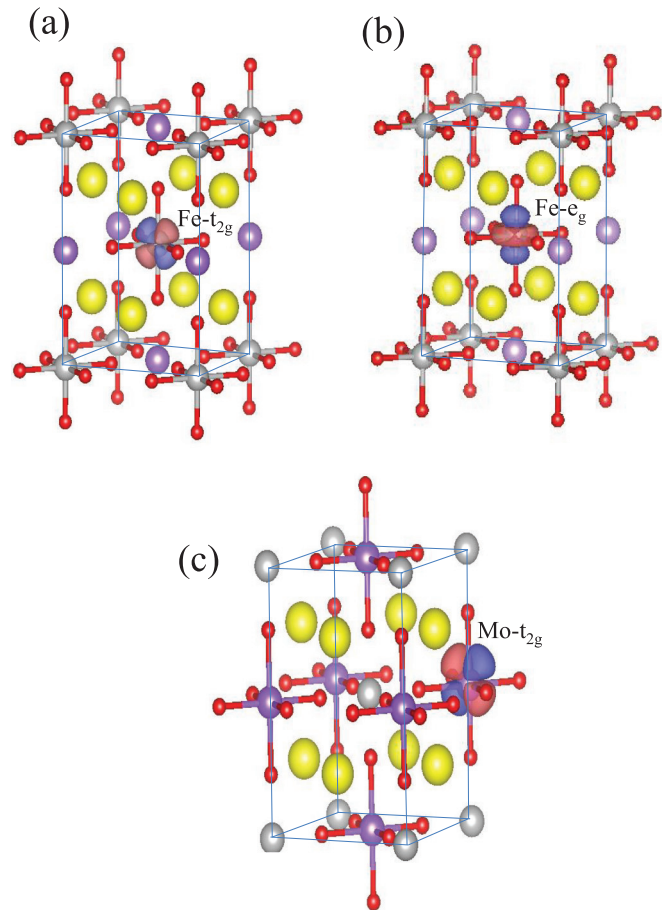

FIG. 3. Fe t_{2g}- and e_g-like and Mo t_{2g}-like Wannier orbitals for nonmagnetic Sr_2FeMoO_6.

There are two parametrizations of this cRPA Coulomb matrix in the static limit ($\omega = 0$) [42,43]. The first is the Hubbard-Kanamori parametrization,

$$U = \frac{1}{L}\sum_{m} U^{\sigma_1\sigma_2}_{mm;mm}, \tag{2}$$

$$U' = \frac{1}{L(L-1)}\sum_{m\neq n} U^{\sigma_1\sigma_2}_{mn;mn}, \tag{3}$$

$$J = \frac{1}{L(L-1)}\sum_{m\neq n} U^{\sigma_1\sigma_2}_{mn;nm}, \tag{4}$$

where L is the number of localized orbitals, i.e., five for d, three for t_{2g}, and two for e_g orbitals. [Henceforth, with U we refer to the average value, Eq. (2), rather than to the matrix, Eq. (1).] If the crystal field has cubic symmetry as in the considered DPs, then the U' is given by $U' = U - 2J$. In this case, only two parameters of U, U', and J are independent, but the Coulomb term of the Kanamori Hamiltonian is still uniquely defined for t_{2g} and e_g subspaces (but not for the d subspace).

The second parametrization is given by

$$U_{\mathrm{S}} = \frac{1}{L^2}\sum_{m,n} U^{\sigma_1\sigma_2}_{mn;mn}, \tag{5}$$

$$J_{\mathrm{S}} = U_{\mathrm{S}} - \frac{1}{L(L-1)}\sum_{m\neq n}\left[U^{\sigma_1\sigma_2}_{mn;mn} - U^{\sigma_1\sigma_2}_{mn;nm}\right]. \tag{6}$$

This parametrization relies on a simplification of the Hubbard Hamiltonian, where the Coulomb interaction is restricted to terms that only contain orbital number operators. To be consistent, we have calculated these parameters for the d and t_{2g} orbitals.

Note that due to the spin dependence of the maximally localized Wannier functions in spin-polarized calculations, the U and J parameters are spin dependent. This effect is negligible in practice. Similarly to U, U', and J, we can also define the so-called fully screened (unscreened) $\tilde{U}$ (V), $\tilde{U}'$ (V'), and $\tilde{J}$ (J_{b}). Although the fully screened Coulomb interaction parameters are not used in model Hamiltonians, they provide an idea about the correlation strength of the considered electrons.

III. RESULTS AND DISCUSSION

This section is divided into two parts. In the first part we briefly discuss the ground-state electronic and magnetic properties of the DPs. The second part deals with a detailed discussion of the effective Coulomb interaction parameters for correlated electrons focusing on the paramagnetic state. The cRPA results will be presented for the two different parametrizations of the Coulomb matrix discussed in the previous section.

A. Ground-state electronic and magnetic properties

We start with a brief description of the ground-state electronic and magnetic properties of the considered DPs. As mentioned in the preceding section, all compounds are assumed to be cubic with lattice constants taken from Ref. [1] and given in Table I. Note that although the low-temperature phase of Sr_2FeWO_6 is in fact insulating [44] with a unit cell composed of 80 atoms, we expect a small influence of this approximation to the obtained U and J values, since the screening channels coming from low-energy excitations (i.e., the ones taking place in the bands of the subspaces) are specifically eliminated in the Hubbard parameters (in contrast to the fully screened parameter, which should be affected more strongly). The different electronic properties of these compounds derive from the crystal field splitting and from the varying occupation of the A- and B-site cations with the increasing band filling from Cr to Ni at the A site. In the first two compounds Sr_2CrBO_6 and Sr_2MnBO_6 the Cr and Mn have a charge valence of 3+ with d^3 and d^4 configuration, respectively, while the formal valence of Fe, Co, and Ni in the next three compounds Sr_2FeBO_6, Sr_2CoBO_6, and Sr_2NiBO_6 are 2+ with d^6, d^7, and d^8 configuration. The largest change in the electronic structure of the DPs is visible in the minority spin channel (see Fig. 4). The minority t_{2g} orbitals are completely empty in the case of Cr at the A site and are found to be completely filled in the case of Ni. At the same time, the minority t_{2g} orbitals of the B-site cation move up in energy from being at the Fermi level in the case of the compounds with Cr at the A site to around 1 eV above the Fermi level in the case of Ni at the A site. Both $Sr_2Mn\{Mo, W\}O_6$ systems are found to be metallic, while the $Sr_2Ni\{Mo, W\}O_6$ ones are found to be insulating. All other compounds are half metallic with a band gap in the majority spin channel. These large changes of the electronic structure with band filling explain the variety of ground states found in these compounds.

In Table I, the atom-resolved as well as the total magnetic moments are reported. The magnetic moments on the A-site cation reflect the expected values due to the increasing occupation of the electronic states, with a maximum around Mn-Fe and a minimum for Ni. On the B-site cation, high negative moments of about -0.5 μ_B are found for $A = $ Cr, Mn, and Fe, which is consistent with a partial filling of the B-site minority t_{2g} orbitals in these compounds. The formal valence of B cations for the first three compounds is 5+ with the d^1 configuration and 6+ (d^0) for the latter cases. These d configurations can describe the small negative moments of B cations in $Sr_2Co\{Mo, W\}O_6$ and $Sr_2Ni\{Mo, W\}O_6$. As the filling of the A-site cation's orbitals increases, the t_{2g} orbitals of the B site are emptied, and the magnetic moments at the B site decrease to a negligible value for Ni. All compounds are ferrimagnetic except the Ni-based ones. Moreover, the total magnetic moments presented in Table I reflect the ground-state properties of the compounds; i.e., for half metals and insulators the total moment assumes integer values, while for the metals it is fractional. Note that interstitial magnetic moments are not shown in Table I.

B. Coulomb interaction parameters

In the model Hamiltonian description of the correlated materials, the noninteracting one-body part of the effective model is defined for a paramagnetic state. The calculation of the effective Coulomb interaction parameters should be based on the same state. As discussed in the preceding section, all DPs can be described by an effective eight-orbital low-energy model, five d orbitals stemming from $3d$ transition

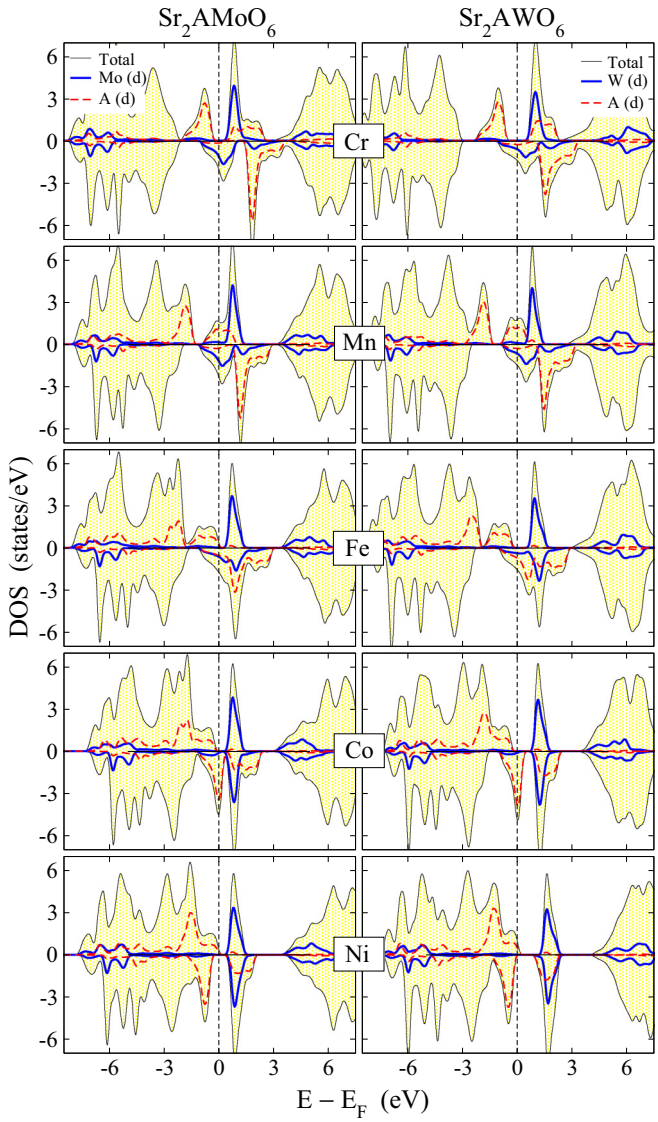

FIG. 4. Spin-polarized density of states (DOS) calculated by DFT-GGA for the double-perovskite series. Each panel shows the total DOS (black lines), the DOS projected onto the A-site cation (dashed red lines), and the DOS projected onto Mo or W (thick blue lines). The Fermi energy is set to zero.

metal atoms (Cr, Mn, Fe, and Co) and three t_{2g} orbitals from Mo (W) atoms, while the Ni-based compounds can even be described by a simpler two-orbital model. In the following, we will discuss effective Coulomb interaction parameters calculated within the cRPA method considering two different parametrizations of the Coulomb matrix.

In Fig. 5, we present the average on-site intraorbital partially screened Coulomb interaction parameters (Hubbard-Kanamori U) for correlated electrons of the ten DPs for the paramagnetic state. For comparison, the corresponding fully screened Coulomb interaction parameters $\tilde{U}$ are also included. As seen, the U values for the $3d$ transition metal atoms (except Ni) slightly increase with increasing electron number. In Mo-based DPs, the U is just above 4 eV, while for W-based compounds it is slightly larger, around 4.5 eV. The slight increase of U from Cr to Co is probably due to

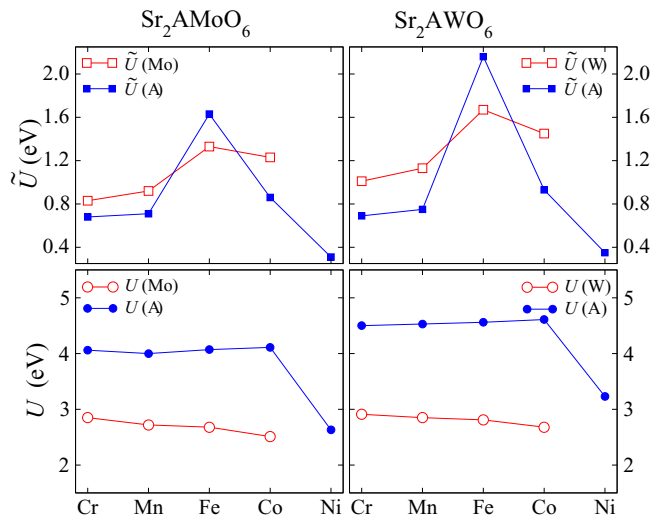

FIG. 5. RPA and cRPA results for the double-perovskite series. The values of the partially screened interaction U (bottom) and the fully screened interaction $\tilde{U}$ (top) for both the A and B sites are presented.

the increased localization of the Wannier functions, which is also reflected by the matrix elements of the unscreened (bare) Coulomb interaction shown in Table II. Indeed, the bare on-site V slightly increases from Cr to Co due to the contraction of wave functions with increasing nuclear charge. Moving from Cr to Co, the existence of d states in the vicinity of E_F leads to a significant effective screening of the d electrons and, as a consequence, to larger $V - U$ differences. The situation for Ni-based compounds is somewhat different. In this case, the obtained U values are about 30%–45% smaller, which is due to the larger number of screening channels contributing to the P_r [see Fig. 2(b)]. In this respect, note that there are no U values for Mo and W atoms for Ni-based DPs, since their subspaces lack corresponding orbitals. For the rest of the compounds, the U values for Mo (W) t_{2g} orbitals are just below 3 eV and slightly decrease from Cr to Co. Although a two-orbital model is more suitable for Ni-based systems, we have, for comparison, also calculated the U parameters using an eight-orbital model and obtained 4.21 eV (4.65 eV) for Ni $3d$ electrons in Sr_2MoNiO_6 (Sr_2WNiO_6). These values are perfectly in line with the trends seen in Table II.

The fully screened on-site $\tilde{U}$ in DPs are much smaller (almost a factor of six) than the partially screened U. Figures 5(a) and 5(b) show a marked maximum of $\tilde{U}$ for the Fe-based compounds. This is due to a small band gap in paramagnetic $Sr_2Fe\{Mo, W\}O_6$, which reduces the screening stemming from the $3d \rightarrow 3d$ and $3d \rightarrow 4(5)d$ channels and which leads to a $\tilde{U}$ value that is larger by more than a factor of two. The $\tilde{U}$ for Mo (W) t_{2g} electrons is slightly larger than the corresponding values for the $3d$ atoms, and it follows the same trend; i.e., it increase slightly with increasing $3d$ electron number.

The calculated U values for Cr, Fe, Mn, and Co (see Fig. 5) are similar to the corresponding values in elementary transition metals [27], while the U values for Mo and W atoms turn out to be smaller. Note again that the U for Ni in $Sr_2Ni\{Mo, W\}O_6$ cannot be directly compared with the

TABLE II. Hubbard-Kanamori parameters [bare V, U, U', and J (in eV)] and parameters according to Eqs. (5) and (6) [U_S, J_S (in eV)] for the two series Sr_2AMoO_6 and Sr_2AWO_6 in paramagnetic state. In parentheses, we present U_S and J_S for the spin-polarized case.

					Sr_2AMoO_6						
A	$V^{[A]}$	$U^{[A]}$	$U'^{[A]}$	$J^{[A]}$	$U^{[Mo]}$	$U'^{[Mo]}$	$J^{[Mo]}$	$U_S^{[A]}$	$J_S^{[A]}$	$U_S^{[Mo]}$	$J_S^{[Mo]}$
Cr	19.54	4.06	2.95	0.53	2.85	2.26	0.27	3.17 (3.26)	0.75 (0.67)	2.46 (2.46)	0.47 (0.47)
Mn	20.31	4.00	2.87	0.55	2.72	2.13	0.27	3.10 (2.86)	0.78 (0.68)	2.33 (2.06)	0.47 (0.48)
Fe	21.62	4.07	2.90	0.57	2.68	2.10	0.26	3.13 (2.89)	0.80 (0.62)	2.29 (2.03)	0.45 (0.46)
Co	21.81	4.11	2.94	0.57	2.51	1.93	0.25	3.17 (2.34)	0.80 (0.58)	2.12 (1.91)	0.44 (0.44)
Ni	18.57	2.14	1.00	0.57				1.57 (1.72)	1.14 (0.86)	(1.78)	(0.41)
					Sr_2AWO_6						
A	$V^{[A]}$	$U^{[A]}$	$U'^{[A]}$	$J^{[A]}$	$U^{[W]}$	$U'^{[W]}$	$J^{[W]}$	$U_S^{[A]}$	$J_S^{[A]}$	$U_S^{[W]}$	$J_S^{[W]}$
Cr	19.87	4.50	3.34	0.57	2.91	2.32	0.28	3.57 (3.64)	0.80 (0.71)	2.52 (2.53)	0.48 (0.47)
Mn	20.60	4.53	3.36	0.59	2.85	2.26	0.27	3.59 (3.31)	0.82 (0.71)	2.46 (2.16)	0.47 (0.48)
Fe	21.89	4.56	3.32	0.61	2.81	2.22	0.27	3.57 (3.53)	0.86 (0.70)	2.42 (2.17)	0.47 (0.47)
Co	21.93	4.61	3.37	0.61	2.68	2.09	0.27	3.62 (2.70)	0.86 (0.61)	2.29 (2.02)	0.47 (0.47)
Ni	18.97	2.99	1.67	0.66				2.33 (2.22)	1.32 (0.95)	(2.06)	(0.43)

corresponding U value in fcc Ni because the subspace of the former is formed only by the e_g states, whereas the one of the latter comprises the full d shell. On the other hand, due to presence of narrow $3d$ ($4d$, $5d$) states around the Fermi level, the $d \rightarrow d$ screening channel is very efficient in the DPs. Therefore, the $\tilde{U}$ values turn out to be quite small. The $\tilde{U}$ parameter varies between 0.3 and 1.6 eV, while in elementary transition metals the corresponding values are around 1–1.5 eV.

For completeness, we present in Table II both Hubbard-Kanamori (U, U', and J) and the parameters defined in Eqs. (5) and (6) (U_S and J_S) for the paramagnetic systems. The latter parameters are also calculated for the spin-polarized case and presented in parentheses. As mentioned in the preceding section, the Hubbard-Kanamori parameters satisfy the $U' = U - 2J$ relation and the Hund exchange J_S is given by $J_S = 1.4J$ due to the cubic symmetry of the systems [45]. The J (J_S) values are less affected by the electronic features and slowly increase for the A-site cation, while remaining rather constant in all cases for the Mo and W cations. This increase can be attributed to the localization of Wannier functions with increasing electron number. For the spin-polarized state, the U parameters show some variations due to the exchange splitting and a redistribution of the states around Fermi energy, but the overall trend is similar to the paramagnetic case for most of the compounds. Note that in the spin-polarized case, the correlated subspace of the Ni-based compounds contains t_{2g} states of Mo (W) atom in addition to the Ni e_g states. The corresponding U_S and J_S values are presented in Table II in parentheses.

Finally, we discuss the frequency dependence of the $U(\omega)$ for the case of Sr_2FeMoO_6, which is certainly one of the most studied DPs [46]. Sr_2FeMoO_6 is an example of a ferrimagnetic half-metallic compound with a Curie temperature well above room temperature, $T_c \simeq 420$ K. In Fig. 6, the frequency-dependent U parameters for Fe d and Mo t_{2g} electrons are presented for the paramagnetic state. At low frequencies, the U values for both Fe and Mo gradually decrease with increasing frequency and present a small spike in the 8–10 eV range, after which the U values show strong fluctuations up to the plasmon frequencies, which are around 25 eV for Fe and 20 eV for Mo. At energies higher than 30–35 eV, the screening becomes ineffective and the effective interaction approaches the bare value, which is about 22 eV for Fe (13 eV for Mo). In the inset, the values for the exchange parameter J are shown. Again, some variations are seen at low energies, before the J parameters reach a relatively constant value above the plasmon frequency, where the value of Fe is about 100% higher than the one of Mo. The presence of large fluctuations in the low-energy regime suggests that the use of the static $U(\omega = 0)$ value might be insufficient to correctly describe low-energy physics, and that a renormalization of the values of U in the low-energy range would be more appropriate.

IV. CONCLUSIONS

We have identified the correlated subspaces in Sr_2ABO_6 (A = Cr, Mn, Fe, Co, Ni, and B = Mo, W) DPs and employed a parameter-free cRPA scheme to calculate the

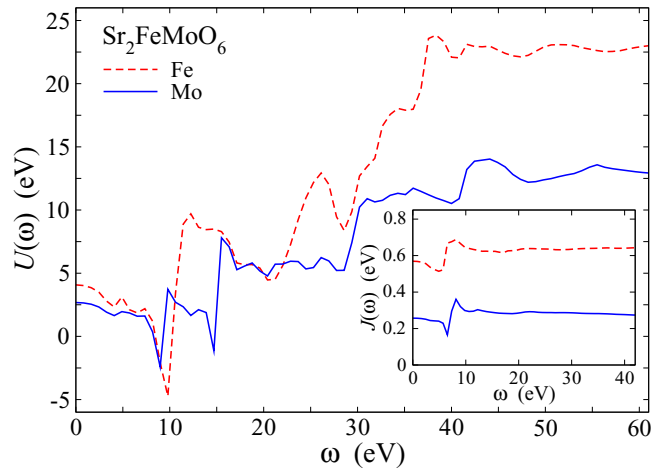

FIG. 6. Frequency dependence of U and J (inset) for Fe $3d$ and Mo t_{2g} electrons in paramagnetic Sr_2FeMoO_6.

effective on-site Coulomb interaction parameters between localized d electrons in these compounds. We find that in the (paramagnetic) Ni-based compounds the correlated subspace can be defined to contain only Ni e_g states, so they can be described by a two-orbital effective low-energy model, whereas for the other compounds at least an eight-orbital ($d + t_{2g}$) low-energy model is necessary. We find that except for Ni, the U values for the A sites in the Mo (W) based compounds are around 4 eV (4.5 eV) and that they are almost independent of the $3d$ electron number, while the U values for Mo (W) t_{2g} electrons slightly decrease with increasing $3d$ electron number, from 3 to 2.5 eV. Moreover, our calculations reveal that the contribution of the $3d \rightarrow 3d$ channel to the total electronic screening is stronger in DPs than in elementary transition metals. The calculated U (J) parameters are not only important for a fundamental understanding of the physics of these compounds, but they can also serve as effective interaction parameters to be used in model Hamiltonians applied to describe electronic, optical, and magnetic properties, thus increasing the predictive power of LDA+U and LDA+DMFT calculations.

ACKNOWLEDGMENTS

Fruitful discussions with G. Bihlmayer and I. Maznichenko are gratefully acknowledged. E.Ş. and I.M. greatly acknowledge the funding provided by the European Union (EFRE, Project No. ZS/2016/06/79307). This work has been supported by the DFG through the Research Unit FOR-1346 and the Young Investigators Group Programme of the Helmholtz Association, Germany, Contract No. VH-NG-409. We gratefully acknowledge the support of the Jülich Supercomputing Centre (Project No. JIFF38). H.H. gratefully acknowledges the support of the Iran Science Elites Federation (Grant No. 66332).

[1] D. Serrate, J. M. De Teresa, and M. R. Ibarra, J. Phys.: Condens. Matter **19**, 023201 (2007).
[2] N. Auth, G. Jakob, W. Westerburg, C. Ritter, I. Bonn, C. Felser, and W. Tremel, J. Magn. Magn. Mater. **272**, E607 (2004).
[3] Y. Krockenberger, K. Mogare, M. Reehuis, M. Tovar, M. Jansen, G. Vaitheeswaran, V. Kanchana, F. Bultmark, A. Delin, F. Wilhelm, A. Rogalev, A. Winkler, and L. Alff, Phys. Rev. B **75**, 020404(R) (2007).
[4] R. N. Mahato, K. Sethupathi, and V. Sankaranarayanan, J. Appl. Phys. **107**, 09D714 (2010).
[5] T. Fukushima, A. Stroppa, S. Picozzi, and J. M. Perez-Mato, Phys. Chem. Chem. Phys. **13**, 12186 (2011).
[6] M. H. K. Rubel, T. Takei, N. Kumada, M. M. Ali, A. Miura, K. Tadanaga, K. Oka, M. Azuma, M. Yashima, K. Fujii, E. Magome, C. Moriyoshi, Y. Kuroiwa, J. R. Hester, and M. Avdeev, Chem. Mater. **28**, 459 (2016).
[7] M. Ležaić and N. A. Spaldin, Phys. Rev. B **83**, 024410 (2011).
[8] W. E. Pickett, Phys. Rev. Lett. **77**, 3185 (1996).
[9] K. Phillips, A. Chattopadhyay, and A. J. Millis, Phys. Rev. B **67**, 125119 (2003).
[10] V. Pardo and W. E. Pickett, Phys. Rev. B **80**, 054415 (2009).
[11] H. Das, P. Sanyal, T. Saha-Dasgupta, and D. D. Sarma, Phys. Rev. B **83**, 104418 (2011).
[12] J. Hong, A. Stroppa, J. Íñiguez, S. Picozzi, and D. Vanderbilt, Phys. Rev. B **85**, 054417 (2012).
[13] A. Cook and A. Paramekanti, Phys. Rev. B **88**, 235102 (2013).
[14] K. Pajskr, P. Novák, V. Pokorný, J. Kolorenč, R. Arita, and J. Kuneš, Phys. Rev. B **93**, 035129 (2016).
[15] Y. P. Liu, H. R. Fuh, and Y. K. Wang, J. Phys. Chem. C **116**, 18032 (2012).
[16] B. C. Jeon, C. H. Kim, S. J. Moon, W. S. Choi, H. Jeong, Y. S. Lee, J. Yu, C. J. Won, J. H. Jung, N. Hur, and T. W. Noh, J. Phys.: Conden. Matter **22**, 345602 (2010).
[17] T. Kotani, J. Phys.: Condens. Matter **12**, 2413 (2000).
[18] I. V. Solovyev and M. Imada, Phys. Rev. B **71**, 045103 (2005).
[19] I. Schnell, G. Czycholl, and R. C. Albers, Phys. Rev. B **65**, 075103 (2002).
[20] P. H. Dederichs, S. Blügel, R. Zeller, and H. Akai, Phys. Rev. Lett. **53**, 2512 (1984).
[21] V. I. Anisimov and O. Gunnarsson, Phys. Rev. B **43**, 7570 (1991); M. Cococcioni and S. de Gironcoli, *ibid.* **71**, 035105 (2005).
[22] K. Nakamura, R. Arita, Y. Yoshimoto, and S. Tsuneyuki, Phys. Rev. B **74**, 235113 (2006).
[23] F. Aryasetiawan, M. Imada, A. Georges, G. Kotliar, S. Biermann, and A. I. Lichtenstein, Phys. Rev. B **70**, 195104 (2004).
[24] F. Aryasetiawan, K. Karlsson, O. Jepsen, and U. Schönberger, Phys. Rev. B **74**, 125106 (2006).
[25] E. Şaşıoğlu, C. Friedrich, and S. Blügel, Phys. Rev. Lett. **109**, 146401 (2012).
[26] T. Miyake and F. Aryasetiawan, Phys. Rev. B **77**, 085122 (2008); T. Miyake, F. Aryasetiawan, and M. Imada, *ibid.* **80**, 155134 (2009).
[27] E. Şaşıoğlu, C. Friedrich, and S. Blügel, Phys. Rev. B **83**, 121101(R) (2011).
[28] T. O. Wehling, E. Şaşıoğlu, C. Friedrich, A. I. Lichtenstein, M. I. Katsnelson, and S. Blügel, Phys. Rev. Lett. **106**, 236805 (2011).
[29] B.-C. Shih, Y. Zhang, W. Zhang, and P. Zhang, Phys. Rev. B **85**, 045132 (2012); B.-C. Shih, T. A. Abtew, X. Yuan, W. Zhang, and P. Zhang, *ibid.* **86**, 165124 (2012); R. Sakuma and F. Aryasetiawan, *ibid.* **87**, 165118 (2013).
[30] H. Sims, W. H. Butler, M. Richter, K. Koepernik, E. Şaşıoğlu, C. Friedrich, and S. Blügel, Phys. Rev. B **86**, 174422 (2012).
[31] Y. Nomura, M. Kaltak, K. Nakamura, C. Taranto, S. Sakai, A. Toschi, R. Arita, K. Held, G. Kresse, and M. Imada, Phys. Rev. B **86**, 085117 (2012); Y. Nomura, K. Nakamura, and R. Arita, *ibid.* **85**, 155452 (2012).
[32] L. Vaugier, H. Jiang, and S. Biermann, Phys. Rev. B **86**, 165105 (2012).
[33] B. Kim, P. Liu, J. M. Tomczak, and C. Franchini, Phys. Rev. B **98**, 075130 (2018).
[34] G. King and P. M. Woodward, J. Mater. Chem. **20**, 5785 (2010).

[35] See http://www.flapw.de.
[36] J. P. Perdew, K. Burke, and M. Ernzerhof, Phys. Rev. Lett. **77**, 3865 (1996).
[37] N. Marzari and D. Vanderbilt, Phys. Rev. B **56**, 12847 (1997).
[38] A. A. Mostofi, J. R. Yates, Y.-S. Lee, I. Souza, D. Vanderbilt, and N. Marzari, Comput. Phys. Commun. **178**, 685 (2008).
[39] F. Freimuth, Y. Mokrousov, D. Wortmann, S. Heinze, and S. Blügel, Phys. Rev. B **78**, 035120 (2008).
[40] C. Friedrich, S. Blügel, and A. Schindlmayr, Phys. Rev. B **81**, 125102 (2010).
[41] E. Şaşıoğlu, A. Schindlmayr, C. Friedrich, F. Freimuth, and S. Blügel, Phys. Rev. B **81**, 054434 (2010).
[42] V. I. Anisimov, I. V. Solovyev, M. A. Korotin, M. T. Czyzyk, and G. A. Sawatzky, Phys. Rev. B **48**, 16929 (1993).
[43] V. Anisimov and Y. Izyumov, *Electronic Structure of Strongly Correlated Materials* (Springer, Berlin, 2010).
[44] L. Jiang, S. V. Levchenko, and A. M. Rappe, Phys. Rev. Lett. **108**, 166403 (2012).
[45] *The LDA+DMFT Approach to Strongly Correlated Materials*, edited by E. Pavarini, E. Koch, D. Vollhardt, and A. Lichtenstein (Forschungszentrum Jülich GmbH, 2011).
[46] K.-I. Kobayashi, T. Kimura, H. Sawada, K. Terakura, and Y. Tokura, Nature (London) **395**, 677 (1998).